

Article

Comprehensive Analysis of the Pollutant Characteristics of Gasoline Vehicle Emissions under Different Engine, Fuel, and Test Cycles

Zongyan Lv ¹, Lei Yang ¹, Lin Wu ^{1,*}, Jianfei Peng ¹, Qijun Zhang ¹, Meng Sun ², Hongjun Mao ^{1,*} and Jie Min ³

¹ Tianjin Key Laboratory of Urban Transport Emission Research, College of Environmental Science and Engineering, Nankai University, Tianjin 300071, China; 15804065543@163.com (Z.L.); 15902251605@163.com (L.Y.); pengjianfeipku@163.com (J.P.); zhangqijun@nankai.edu.cn (Q.Z.)

² Tianjin Eco-Environmental Monitoring Center, Tianjin 300071, China; sunm1127@163.com

³ Tianjin SwARC Automotive Research Laboratory Co., Ltd., Tianjin 300071, China; jie.min@swarc.com.cn

* Correspondence: wulin@Nankai.edu.cn (L.W.); hongjunm@Nankai.edu.cn (H.M.); Tel.: +86-22-18630810590 (L.W.); +86-22-186022187891 (H.M.)

Abstract: Vehicle exhaust emissions have seriously affected air quality and human health, and understanding the emission characteristics of vehicle pollutants can promote emission reductions. In this study, a chassis dynamometer was used to study the emission characteristics of the pollutants of two gasoline vehicles (Euro 5 and Euro 6) when using six kinds of fuels. The results show that the two tested vehicles had different engine performance under the same test conditions, which led to a significant difference in their emission characteristics. The fuel consumption and pollutant emission factors of the WLTC cycle were higher than those of the NEDC. The research octane number (RON) and ethanol content of fuels have significant effects on pollutant emissions. For the Euro 5 vehicle, CO and particle number (PN) emissions decreased under the WLTC cycle, and NO_x emissions decreased with increasing RONs. For the Euro 6 vehicle, CO and NO_x emissions decreased and PN emissions increased with increasing RONs. Compared with traditional gasoline, ethanol gasoline (E10) led to decreases in NO_x and PN emissions, and increased CO emissions for the Euro 5 vehicle, while it led to higher PN and NO_x emissions and lower CO emissions for the Euro 6 vehicle. In addition, the particulate matter emitted was mainly nucleation-mode particulate matter, accounting for more than 70%. There were two peaks in the particle size distribution, which were about 18 nm and 40 nm, respectively. Finally, compared with ethanol-gasoline, gasoline vehicles with high emission standards (Euro 6) are more suitable for the use of traditional gasoline with a high RON.

Keywords: chassis dynamometer; ethanol gasoline; research octane number; pollutant emissions; particle size distribution



Citation: Lv, Z.; Yang, L.; Wu, L.; Peng, J.; Zhang, Q.; Sun, M.; Mao, H.; Min, J. Comprehensive Analysis of the Pollutant Characteristics of Gasoline Vehicle Emissions under Different Engine, Fuel, and Test Cycles. *Energies* **2022**, *15*, 622. <https://doi.org/10.3390/en15020622>

Academic Editors: Yuhan Huang and Constantine D. Rakopoulos

Received: 30 November 2021

Accepted: 20 December 2021

Published: 17 January 2022

Publisher's Note: MDPI stays neutral with regard to jurisdictional claims in published maps and institutional affiliations.



Copyright: © 2022 by the authors. Licensee MDPI, Basel, Switzerland. This article is an open access article distributed under the terms and conditions of the Creative Commons Attribution (CC BY) license (<https://creativecommons.org/licenses/by/4.0/>).

1. Introduction

With the development of the economy and industrialization, the automobile industry is developing rapidly. In 2019, the number of motor vehicles in China reached 348 million, of which gasoline vehicles accounted for 74.7% (260 million). Simultaneously, the pollution caused by the transportation sector has become increasingly prominent and has become the primary source of air pollution in most of China's urban areas. People are paying more and more attention to the environmental problems caused by traffic. Reducing vehicle emissions is very important for alleviating air pollution [1].

Exhaust pollutants are produced during the operation of automobile engines. Studies have shown that fuel composition and engine settings significantly affect fuel economy, gaseous emissions, and particulate matter (PM) emissions [2–4]. The differences in gasoline engines are mainly reflected in the fuel injection strategy, compression ratio, speed, load, and other parameters. The differences of gasoline are manifested in the octane number, sulfur

content, distillation range, and so on. Gasoline is a complex manufactured mixture made up of hydrocarbons, additives, and blends [5]. The octane number of the gasoline is one of the most important parameters describing the anti-knocking quality of fuel, and it has a significant impact on engine efficiency and emissions [6,7]. The optimal octane number of gasolines is determined by the engine design and the compression ratio. Generally, high-octane fuel makes the engine perform better. Sayin et al. tested the influence of two gasoline fuels with different octane numbers, RON91 and RON95, on engine performance and emissions [6]. The results showed that RON91 fuel had lower CO and HC emissions. Moreover, Liu et al. investigated the impact of the octane number (ON) on the combustion and emissions of an HCCI engine and found that high-octane fuels tended to emit more CO and HC [8].

E10 is a gasoline ethanol blend with up to 10 vol% ethanol, and China has been advancing the popularity of ethanol gasoline. Many studies have shown that ethanol fuels result in the reductions of total hydrocarbon (THC), nitrogen oxide (NO_x), and carbon monoxide (CO) emissions from vehicles [9–12]. Some studies have also found that ethanol–gasoline can effectively reduce particulate matter emission in the tail gas [5,13–16]. The reduction in particulate matter caused by ethanol fuel can be attributed to the chemically bonded oxygen and the OH bond, which promote oxidation of the precursors [17–20]. However, some studies have shown that ethanol–gasoline leads to higher particulate emissions [21–24]. Chen et al. studied the effect of ethanol content on particulate emissions from a single-cylinder GDI engine. PN emissions increased when ethanol content increased. The author suggested that the number of particles increases because the high evaporation enthalpy of ethanol fuel makes it difficult for the fuel to evaporate completely during the injection process, resulting in higher particle number emissions.

Besides this, some studies showed that increased aromatics content would lead to increases in carbon monoxide (CO), total hydrocarbons (THC), particulate matter mass, and particle number [25–27]. Zhu et al. found that aromatic and olefin contents had relatively small impacts on fuel consumption [28]. Yang et al. studied the effects of varying aromatic contents (20% and 30%) on the direct injection exhaust emissions of five vehicles. They found that aromatics played an essential role in the emissions, but aromatics had no effect on NO_x emissions [29]. Schifte et al. studied the influence of the olefin and aromatic content of gasoline on exhaust emissions with 15% ethanol blends. They found that non-oxygenated fuels with a high aromatic and olefin content showed higher ozone formation values, and the aromatic content was positively related to hydrocarbons and CO₂ emissions [30]. Other studies have also shown the strong influence of gasoline aromatics on GDI and PFI vehicles [31–33].

Many factors besides fuel affect automobile emissions, such as engine technology, driving conditions, and post-processing technology. Among these, engine technology is the principal influence. At present, gasoline direct injection (GDI) and port fuel injection (PFI) are the two main fuel injection technologies. Although PFI vehicles now make up most of China's vehicle fleet, the proportion of GDI vehicles is increasing rapidly. GDI engines can effectively improve the gasoline engine's compression ratio and thermal efficiency, and are widely available worldwide. In Europe, for example, more than 40% of light vehicles are equipped with GDI engines [34]. However, a light-duty vehicle with a GDI engine tends to emit more particulate matter (PM) (especially particle numbers (PNs)) compared with port fuel injection (PFI) vehicles and diesel engines equipped with particle filters (e.g., diesel particulate filters, DPF) [35]. Many studies have indicated that particle numbers emitted from GDI engines cannot meet the emission limits mandated by the China 6 regulations— 6×10^{11} #/km. Studies have explained why GDI PN emissions are high due to the uneven mixing of fuel and air. The PN emissions of GDI engines have attracted widespread attention, and more and more people are studying this [36,37], especially tiny particles. At the same time, some roadside observation experiments found that the particulate matter emitted by traffic sources is an important part of atmospheric aerosols [38,39]. Because the discharged particles are all small-sized particles, they account for a relatively low proportion of the quality of particles, but a large proportion in the

quantity. Although particle emissions from gasoline vehicles are of increasing concern, relevant studies on this issue are lacking.

In the 1990s, the European Union launched its automotive emission regulations [40]. Since then, other countries have begun to follow suit, and some countries have directly adopted the European automotive emission regulations. Increasingly stringent emission regulations continue to reduce pollutant limits. China announced the China 6 regulations in 2016, and these regulations were fully implemented nationwide in July 2020. The NEDC (New European Driving Cycle) and WLTC (Worldwide harmonized Light vehicles Test Cycles) tests are the most widely used test cycles for light vehicles in China. The NEDC cycle includes four urban driving segments (UDC) characterized by low vehicle speeds, low engine loads, and low exhaust gas temperatures, followed by one extra-urban driving segment (EUDC) to account for more aggressive and high-speed driving modes. The WLTC consists of four-speed phases (low, medium, high, and extra-high). The average speed and maximum speed of the NEDC are 33.6 km/h and 120 km/h, respectively, while the average speed and maximum speed of the WLTC are 46.5 km/h and 131.3 km/h, respectively. Because the WLTC can better reflect real road conditions, the China 6 regulation required the WLTC to replace the NEDC, which is not representative for assessing compliance with pollutant emission limitations and vehicle fuel economy requirements [41]. Many studies have compared the two test cycles and verified them [42–46].

The objective of this study was to investigate the effects of engine operation characteristics, gasoline research octane numbers (RONs), and ethanol levels on the fuel economy and emissions of two GDI vehicles (Euro 5 and Euro 6) over the NEDC and WLTC test cycles. This study mainly analyzed the impact on gas emissions, and discussed particle number concentration and PSD. In this work, previous studies were verified and further supplemented.

2. Materials and Methods

2.1. Test Fuel Types

At present in China, many areas have begun to sell ethanol gasoline (E10) to replace traditional gasoline. Six fuels were used in this study. The physical and chemical properties of the fuels are given in Table 1. All the fuels were prepared by a specific supplier in accordance with China's standards for motor vehicle gasoline. The six gasolines have been labeled as G1, G2, E1, G3, G4, and E2. The fuel number indicates the RON and ethanol content of each gasoline type. Of these types of gasoline, four are conventional gasolines (G1, G2, G3, and G4), and two are ethanol gasolines (E1 and E2). Ethanol-gasoline is a blend of 90% regular gasoline and 10% ethanol fuel.

Table 1. Parameters of the tested fuels.

Fuels	G1	G2	E1	G3	G4	E2	Test Method
Research octane number (RON)	92.6	92.4	92.7	95.4	95.3	96.1	GB/T 5487
Sulfur (mg/kg)	6.3	4.2	6.3	6.2	5	6.5	SH/T 0689
Density, @20 °C (kg/m ³)	733.5	741.2	734.3	738.6	746.5	734.3	GB/T 1884
Vapor pressure (kPa)	58.6	61	61	58.1	60.2	60.1	GB/T 8017
Olefin (V/V)	9.1%	14.1%	11.3%	9%	14%	10.6%	SH/T 0741
Benzene (V/V)	0.6%	0.5%	0.7%	0.6%	0.5%	0.7%	SH/T 0713
Aromatics (V/V)	23%	28.2%	28.4%	25%	32.1%	29.1%	SH/T 0741
Ethanol (m/m)	-	-	10.5%	-	-	10.9%	SH/T 0663
Methanol (m/m)	0.1%	0.1%	-	0.1%	0.1%	-	SH/T 0663

As shown in Table 1, G1, G2, and E1 have a lower RON. As is known to all, the higher the octane number is, the better the anti-explosion performance of the engine. Of the gasoline types with low RONs, G1 has the highest sulfur content, G2 has the lowest, and G1 and E1 have a similar sulfur content. Correspondingly, for high RON gasoline, G3 has the highest sulfur content, G4 has the lowest, and G3 and E2 have a similar sulfur content. In terms of olefin content, G2 and G4 are the highest, followed by E1 and E2, then the other gasoline types.

2.2. Test Vehicle

Urban vehicles are mainly light gasoline vehicles, and most of them are vehicles meeting the Euro 4 and Euro 5 emission standards. With the implementation of the Euro 6 emission standards, the proportion of Euro 6 compliant vehicles is gradually increasing. Therefore, two conventional gasoline vehicles (Euro 5 and Euro 6) were selected in this study: the technical specifications of the test vehicles are described in Table 2. Both vehicles were rented from an external provider and are considered typical of the Chinese fleet in their categories. To ensure that the experiment ran smoothly, we carried out a comprehensive inspection of the test vehicles. The vehicles were numbered according to the emission standards (#1 and #2).

Table 2. Specifications of test vehicles.

	Vehicle #1	Vehicle #2
Registration year	2017	2019
Emission standard	Euro 5	Euro 6
Length × width × Height	4620 × 1775 × 1480	4695 × 1885 × 1700
Wheelbase (mm)	2700	2710
Intake system	VGA, VVT-iW	VGA, DCVVT
Cylinders	Inline, 4	Inline, 4
Displacement (mL)	1197	1495
Compression ratio	10	10
Maximum torque (N·m)	185	265
Maximum power (kW)	85	112
Odometer (km)	29,000	20,000
After-treatment configuration	TWC	TWC

2.3. Test Cycles

The test cycles were the NEDC (New European Driving Cycle) and the WLTC (Worldwide harmonized Light vehicles Test Cycles). The WLTC has the vehicle accelerating or decelerating 84% of the time over the whole cycle, with only 13% at idle and 4% driving at a constant cruise. In comparison, 40% of the NEDC is at steady-state cruise conditions, 24% is at idle, and 36% involves accelerating or decelerating [43,45–47]. To explore the two test cycles profoundly, Figure S2 presents the acceleration distribution in terms of velocity for both test cycles. The NEDC only has a few constant accelerations and decelerations at different velocities, and the value is simplex. In contrast, the WLTC covers a wider band of combinations, and it has sufficient combinations of acceleration and vehicle speeds to reflect a vehicle's actual on-road conditions effectively.

2.4. Instrumentation

In this study, a SEMTECH-DS PEMS system (manufactured by Sensors Inc., Saline, MI, USA) was used to measure gaseous pollutant emissions. The system consisted of an exhaust flow meter (EFM), a heated sampling tube, exhaust gas analyzers, a global positioning system (GPS), and a weather station for recording ambient temperature and humidity. The SEMTECH-DS utilized a NDIR (non-dispersive infrared) method to measure the exhaust gas concentrations of CO (carbon monoxide) and CO₂ (carbon dioxide), a NEUV (non-dispersive ultraviolet) method to measure NO_x (nitrogen oxide), and a flame ionization detector (FID) system to measure THC (total hydrocarbons). The data on pollutants were recorded at 1 Hz frequency. The EFM used a pitot tube based on Bernoulli's principle to calculate the mass flow on the basis of the air flow differential pressure measurement [48]. Before the test, the analyzer was calibrated with nitrogen and standard gas to ensure its accuracy.

An electrical low-pressure impactor (ELPI), manufactured by Dekati Ltd. (Kangasala, Finland), was used to measure the particle concentration and size distribution as a function of the aerodynamic particle size in real-time in this study. Many articles have described the performance and usage of these instruments [49–53]. The instrument used in this

study was a high-temperature electrical low-pressure impactor (HT-ELPI+), which is a unique version of the Dekati ELPI+. It enables real-time measurement of particles with a size distribution from 0.006 μm to 10 μm , and the particle size range covers five orders of magnitude, including most nucleation-mode particles ($D_p < 50 \text{ nm}$) and all accumulation-mode particles ($50 \text{ nm} < D_p < 1000 \text{ nm}$) [54,55]. The HT-ELPI+ allows direct measurement of high-temperature (up to 180 $^{\circ}\text{C}$) aerosol samples without cooling the sample, which can prevent the generation of new particles.

2.5. Study Design of the Experiment

Two vehicles were tested using the six fuels on a vehicle chassis dynamometer. A schematic diagram of the experimental system is shown in Figure S1. Each test consisted of 3 NEDC cycles and 3 WLTC cycles, with a specific interval between each test cycle. To ensure the consistency of the measurements to eliminate the influence of confounding factors, the residual gasoline was burned up before switching to the next fuel. After the new fuel had been added, the vehicle was driven through a test NEDC cycle to ensure that the fuel supply system was full of fresh fuel. In the process of the test, the vehicle was driven by computer software controlling the throttle voltage based on the test conditions, which ensured that the driving conditions of each type of cycle were consistent. In addition, we conducted more than two tests on each fuel and each working condition.

2.6. Data Quality Assurance

Measured data include 1 Hz data from the PEMS, OBD data logger. Negative values of concentrations typically occurred when the real pollutant concentration was low and not statistically significantly different from zero. In such cases, the negative values were set to zero or excluded. The exhaust flow rates can be directly measured using an exhaust flow meter. The fuel use rate based on mass per time-based fuel use and the exhaust emission rates for each second were estimated based on the estimated exhaust flow rate and the measured pollutant concentrations. To mitigate against measurement errors, the PEMS was span-calibrated to standard gas mixtures before each measurement.

3. Results and Discussion

3.1. Engine Performance of the Test Vehicles

This section discusses the operating characteristics of the engines of the test vehicles under different test cycles. The engine's operating characteristics have a great impact on emissions [56,57]. Figure S3 gives the time-domain profiles of the vehicles (speed and acceleration) and engines (speed and load). It presents the relationships between the vehicle's speed and acceleration, engine speed, and the two vehicles' load for two test cycles. When the vehicle was idle (speed = 0, acceleration = 0), the engine speed and load are in a low steady-state. Under cruise mode (speed is a constant but not 0, acceleration = 0), the engine speed and load were in a higher steady-state.

Figure 1 illustrates the engine speed and load of the two vehicles during the two test cycles. Figure 1a shows the distribution of engine speed and load. Both the engine speed and the load of Vehicle #1 were to the left of those of Vehicle #2. Figure 1b illustrates the statistical distribution of the engine speed and load of the test vehicles during different cycles. It shows the difference in the speed and load between the two vehicles during the two test cycles. Vehicle #1's engine speed was mostly distributed between 810 and 1630 rpm in the NEDC and between 830 and 2150 rpm in the WLTC, while the engine speed of Vehicle #2 was mainly distributed between 810 and 2000 rpm in the NEDC, and between 810 and 2330 rpm in the WLTC. For the engine load, the main distribution range was 15–48% in the NEDC, and 13–63% in the WLTC for Vehicle #1, and 13–41% in the NEDC, 12–52% in the WLTC for Vehicle #2. Compared with Vehicle #1, Vehicle #2 had a higher engine speed and a lower engine load within the same test cycle. Both vehicles had a higher engine speed and a higher engine load during the WLTC cycle.

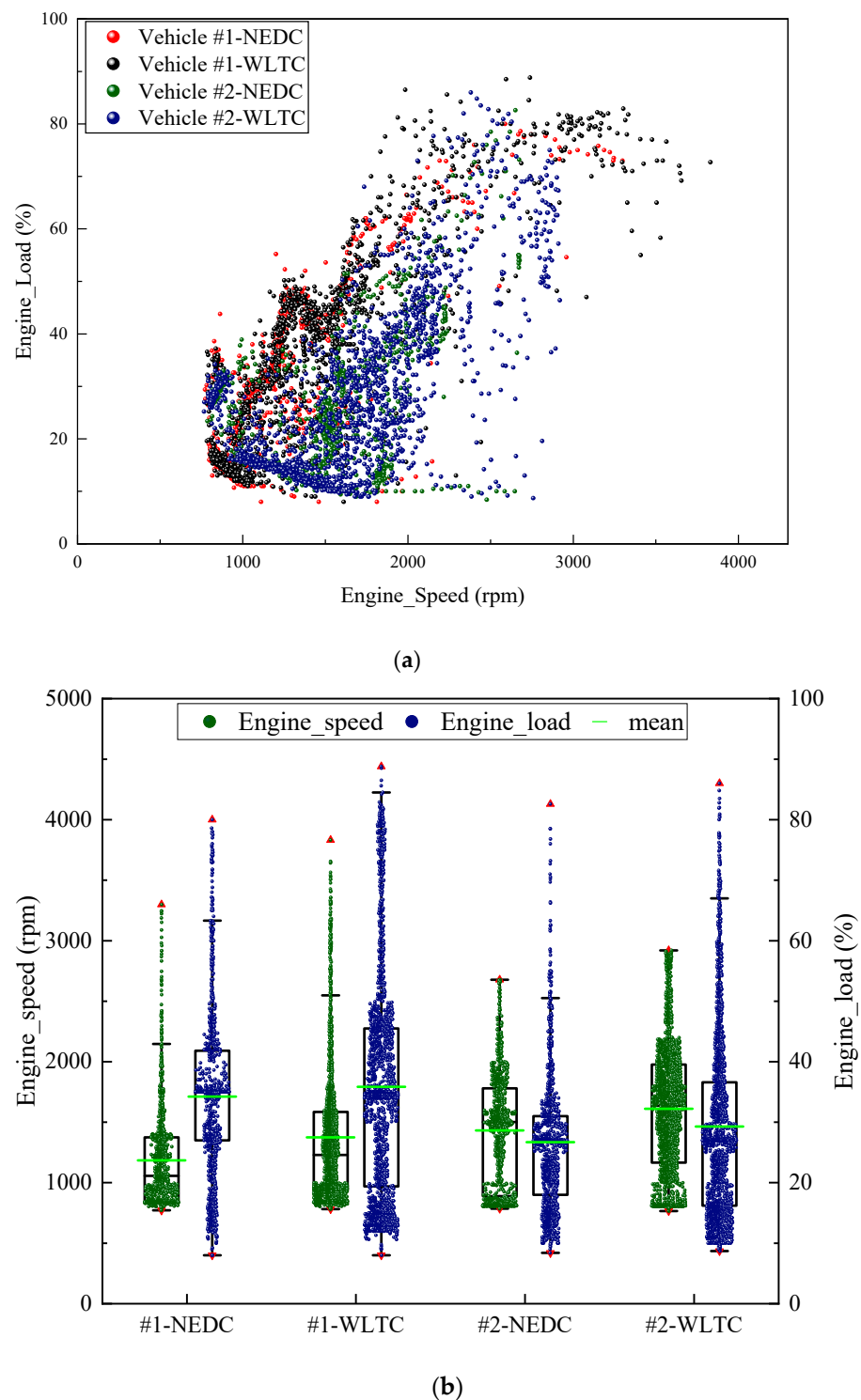


Figure 1. Engine speed vs. load distribution of the two test vehicles: (a) distributions of engine speed and load; (b) statistical distributions of engine speed and load.

3.2. CO₂ Emissions and Fuel Economy

Figure S4 illustrates the evolution of the two vehicles' instantaneous CO₂ emissions during the NEDC and WLTC test cycles using six different fuels. There is a good correlation between CO₂ emissions and vehicle speed. The CO₂ emissions peak appears in the acceleration section. This is because of the increase in engine speed and load during the acceleration phase. When the acceleration stopped, CO₂ emissions dropped sharply to a lower value. In the NEDC cycle, the maximum instantaneous CO₂ emissions occurred

during the EUDC cycle, that is the vehicle was moving at that speed to its maximum value. It is also the time when engine speed and load reached the maximum. The instantaneous emissions of vehicles were stable during idling and at constant-speeds, and decreased when the vehicles slowed down. In the last section, engine speed and load had a similar variation. From this, we can see CO₂ emissions mainly depend on the vehicle's engine speed and load. Figure S5 illustrates the evolution of the instantaneous fuel consumption (FC) rate. The change in instantaneous fuel consumption with velocity was similar to that of CO₂. The peak of the instantaneous fuel consumption rate also appeared in the acceleration section because of the increase in engine speed and load during the acceleration phase.

Figures 2 and 3 show the specific CO₂ emissions and fuel consumptions of the six fuels during the NEDC and WLTC. There is a typical linear relationship between fuel consumption and CO₂ emissions. Wang et al. quoted someone else's formula for calculating fuel consumption, and the coefficient between CO₂ emissions and fuel consumption was around 23.2 (100 g/L) [47]. In this study, the coefficient was 23.8 and 23.7 for Vehicle #1 and Vehicle #2, respectively.

For both test vehicles, the fuel consumption during the WLTC was higher than that during the NEDC. For Vehicle #1, there was a significant difference in fuel consumption between the NEDC and WLTC. The most notable difference appeared for G4, for which the WLTC rate was 8.44% higher than that of the NEDC. The specific fuel consumptions during the WLTC were, on average, 6.60% higher than that during the NEDC for Vehicle #1, but for vehicle #2, the difference in fuel consumption between the NEDC and WLTC was minimal. The difference between the two conditions was the largest for G4 among all the test fuels, for which consumption during the WLTC was 2.01% higher. The WLTC used an average of 2% more fuel than the NEDC for Vehicle #2. For these two vehicles, the average engine load of Vehicle #2 was smaller for both cycles, resulting in a small difference in fuel consumption.

When traditional gasolines were used, a higher RON resulted in a lower FC. This result was consistent with the results by Stradling et al. [58]. When Vehicle #1 switched from conventional gasoline to ethanol, the FC did not change significantly. However, for Vehicle #2, the FC of E2 fuel was higher than that of other fuels. The content of the other fuel components (olefins, benzene, and aromatics) was too low to reflect their importance to FC. Obviously, the fuel consumption of Vehicle #2 was significantly higher than that of Vehicle #1. This may be because the average engine speed of Vehicle #2 was higher than that of Vehicle #1, resulting in a higher fuel injection rate for Vehicle #2, resulting in higher fuel consumption.

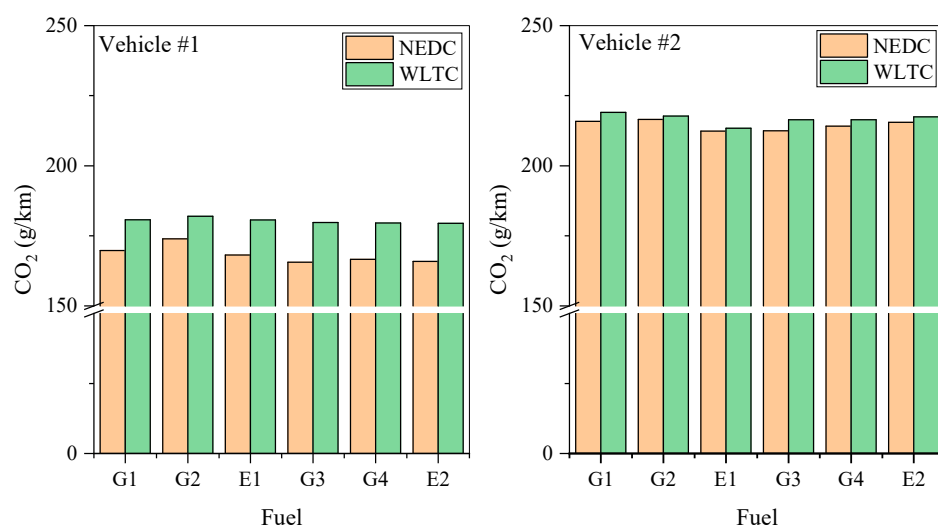


Figure 2. Specific CO₂ for the six fuels.

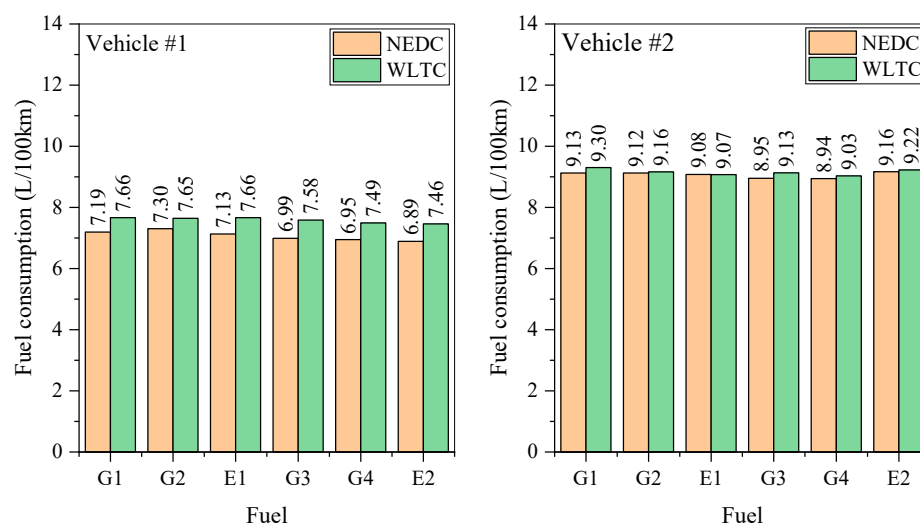


Figure 3. Specific fuel consumption rates for the six fuels.

3.3. CO and NO_x Emissions

Figure S6 shows the instantaneous emissions of CO from the two vehicles during the NEDC and WLTC test cycles using the six fuels. The CO emissions increased significantly as the vehicle speed increased (the acceleration phase). Because the fuel injection increased, the air–fuel ratio decreased, and the combustion was incomplete during the acceleration stage. The emissions were remarkably high during high-speed acceleration during the NEDC (in the EUDC stage) and the WLTC (in the ultra-high stage). The instantaneous emissions value of CO in the ultra-high stage of the WLTC was higher than that at the EUDC stage of the NEDC for the two test vehicles.

Figure 4 gives the specific CO emissions (g/km) of the two vehicles for each fuel type during the NEDC and WLTC test cycles. For Vehicle #1, the EF of CO during the WLTC was higher than that during the NEDC cycle, and high-RON fuels emitted more CO. CO emissions during the WLTC were 97%, 93%, 116%, 104%, 91%, and 105% higher than those of the NEDC for six test fuels, respectively. Unlike Vehicle #1, low-RON fuels had higher CO EF for Vehicle #2. Moreover, the EF of CO during the WLTC was not always higher than that during the NEDC when using different fuels. Because ethanol fuel is oxygen-rich, it could reduce carbon monoxide emissions. However, the carbon monoxide emissions of gasoline vehicles using ethanol–gasoline were higher than those of vehicles using traditional gasoline. Obviously, under NEDC conditions, the emissions of Vehicle #2 are higher than that of Vehicle #1. This may be due to the high fuel consumption of Vehicle #1.

The instantaneous NO_x emissions of the six fuels during the two cycles for the two vehicles are presented in Figure S7. NO_x emissions increased when the vehicle accelerated, and the peaks appeared at the end of the acceleration phases. When a vehicle accelerates, the amount of fuel injection increases and the cylinder’s temperature rises, resulting in higher NO_x emissions. NO_x emissions go up sharply during high-speed acceleration in the NEDC (at the EUDC stage) and WLTC (at the ultra-high stage).

Figure 5 compares the specific NO_x emissions of the six fuels during the NEDC and WLTC cycles for the two vehicles. The specific NO_x emissions of the WLTC cycle are higher than those of the NEDC for the two test vehicles. As we know, NO_x is generated in a high-temperature and oxygen-rich environment. Compared with the NEDC cycle, vehicles had higher average engine speed and load during the WLTC, leading to a relatively long period of high temperatures, which contributed to increasing the NO_x emissions. Low-RON gasoline emitted more NO_x, which is because low-octane fuels cause strong knocking. For Vehicle #1, the WLTC NO_x emissions were 120%, 109%, 145%, 109%, 69%, and 137% higher than those of the NEDC for the six test fuels, respectively. For Vehicle #2, the WLTC NO_x emissions were 50%, 30%, 51%, 5%, 17%, and 75% higher than those of the

NEDC for the six test fuels, respectively. Because ethanol fuel is oxygen-rich, it will emit more NOx. Vehicle #2 is fully compliant but not Vehicle #1. Not all vehicles will reduce emissions when using ethanol–gasoline.

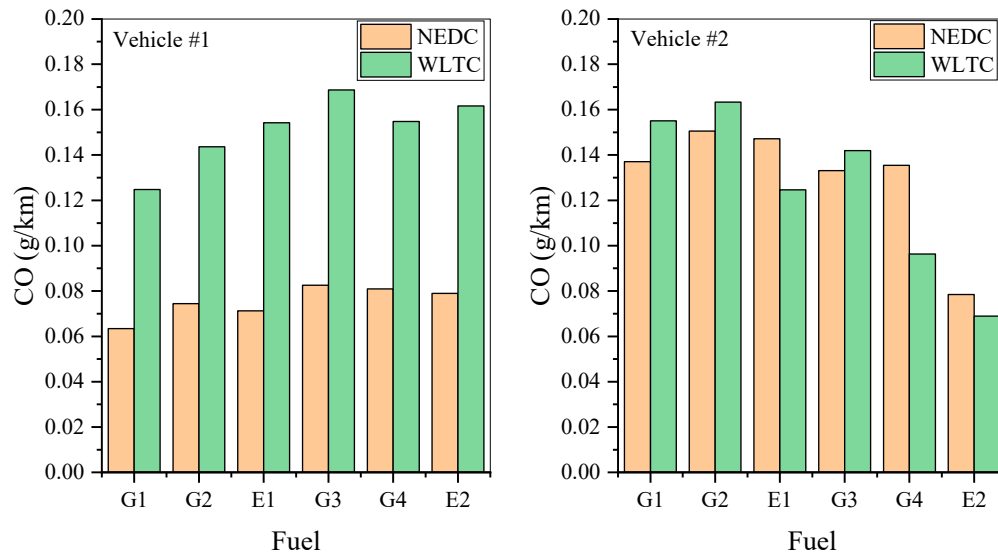


Figure 4. Specific CO emission for the six fuels.

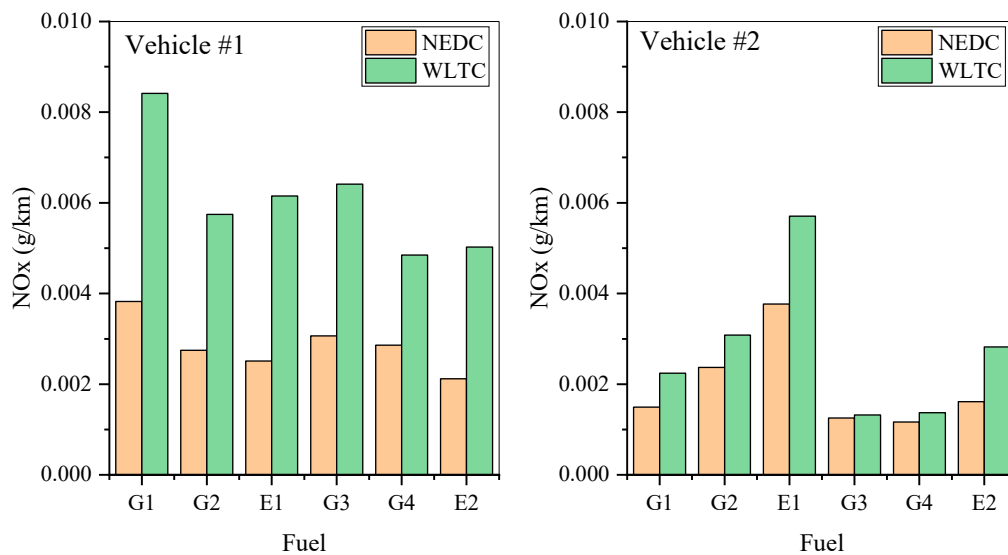


Figure 5. Specific NOx emission for the six fuels.

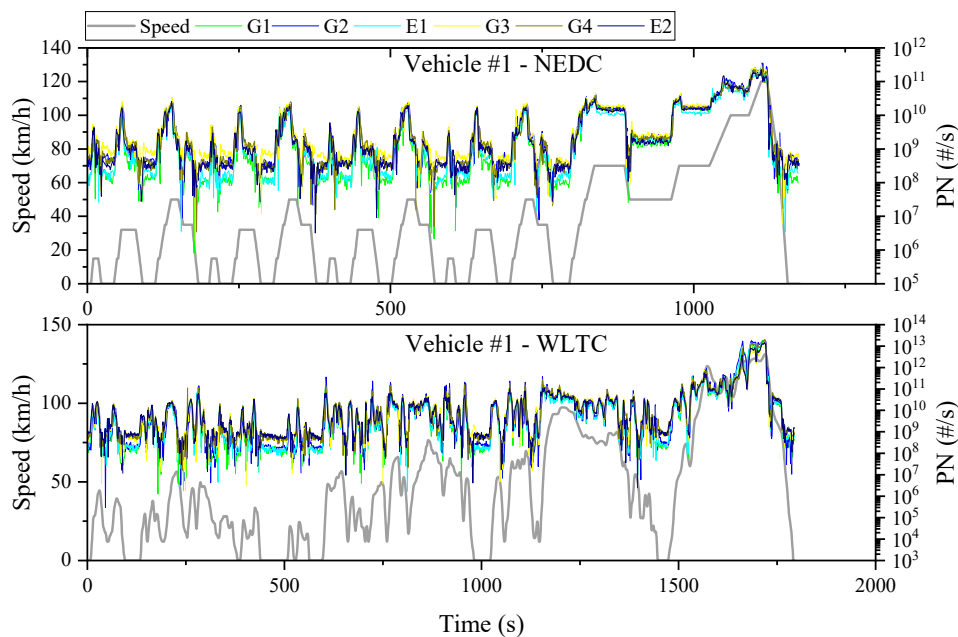
3.4. Particle Number Emissions

3.4.1. Particle Number Emissions

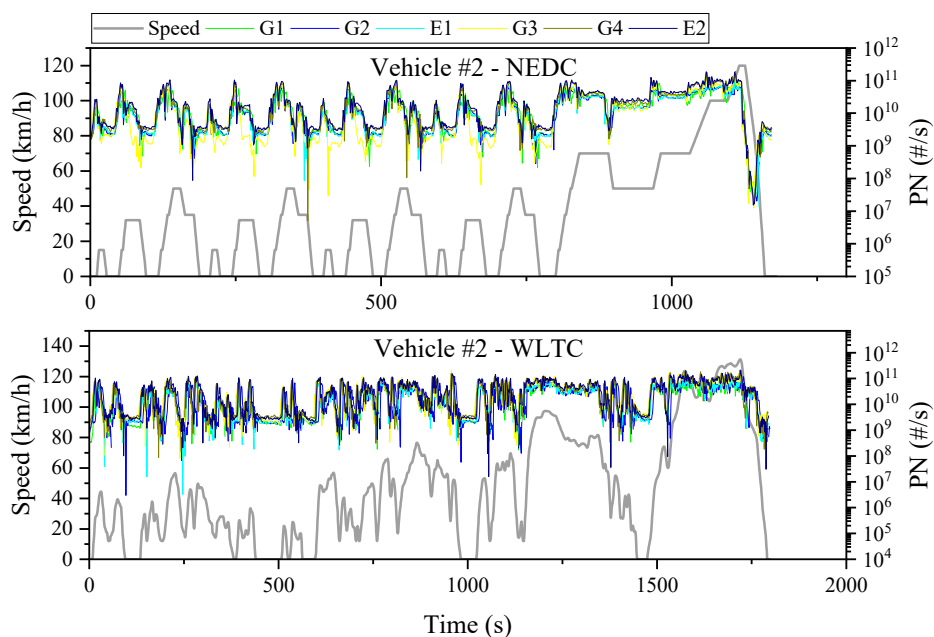
The instantaneous total particle number concentrations of the two test vehicles are shown in Figure S8. The particle number concentration increased sharply with vehicle velocity. Significant peaks of particle numbers were located at the end of the acceleration phase. For Vehicle #1, the particle number concentration was between 10^5 #/cm³ and 10^8 #/cm³ in the NEDC cycle, and between 10^6 #/cm³ and 10^{10} #/cm³ in the WLTC cycle. For Vehicle #2, the particle number concentration was between 10^5 #/cm³ and 10^8 #/cm³ in the NEDC cycle, and between 10^6 #/cm³ and 10^8 #/cm³ in the WLTC cycle. For the two vehicles, the particle number concentration was rarely observed during idling. The difference in particle number concentrations at each cruising speed is tiny in Vehicle #2. This might be because the engine load of Vehicle #2 changed little at different cruising speeds.

For Vehicle #1, there was a lower particle number concentration when the lower-octane fuels were burnt, but the opposite is true for Vehicle #2.

Figure 6 plots the time evolution of the total particle numbers. The number of particles per second is multiplied by the concentration per second in the corresponding exhaust volume flow. For Vehicle #1, the particle numbers were between 10^6 #/s and 10^{11} #/s in the NEDC cycle, and between 10^6 #/s and 10^{13} #/s in the WLTC cycle. For Vehicle #2, the particle numbers were between 10^7 #/s and 10^{11} in both the NEDC and WLTC test cycle.



(a)



(b)

Figure 6. Instantaneous particle number emissions from the two vehicles during the NEDC and WLTC tests with different fuels: (a) Vehicle #1; (b) Vehicle #2.

When the vehicle is at a high speed (EUDC phase in the NEDC and extra-high-speed phase in the WLTC) the engine speed and load are at a higher level, and the combustion time of fuel becomes shorter. The particle number increases sharply with incomplete combustion. When the vehicle accelerates, the inlet pipe pressure rises and more gasoline is needed to achieve better power, which leads to an increase in fuel consumption. Hence, the engine generates more particulate matter.

3.4.2. PN EFs

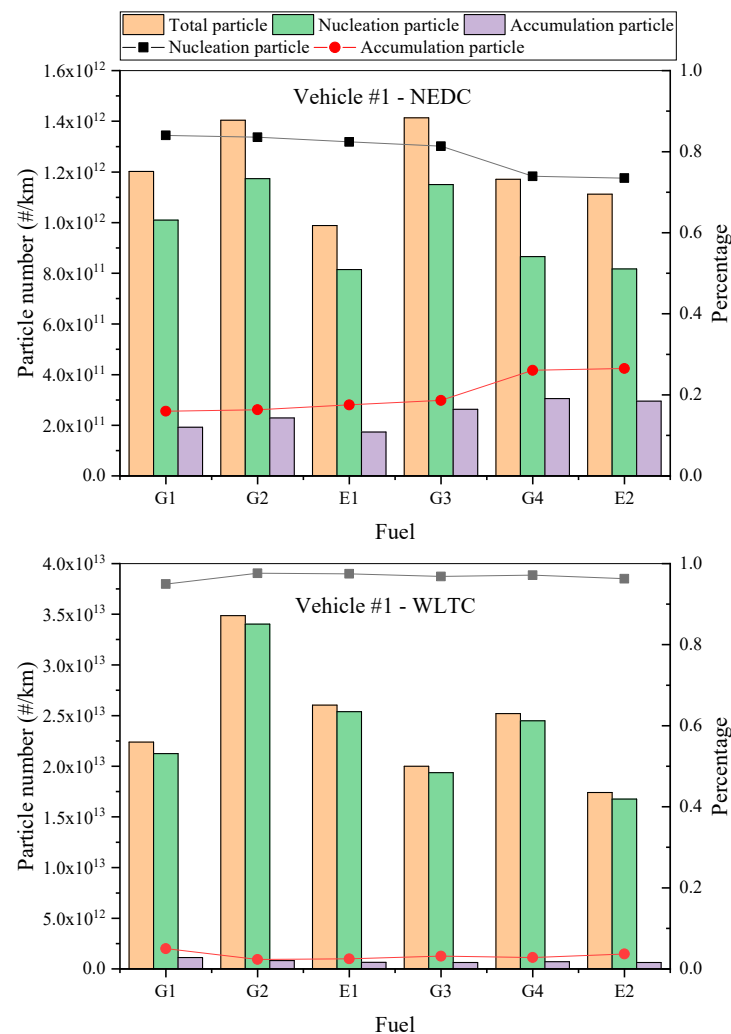
Figure 7 shows the emission factors of the particle numbers of the two test vehicles with six fuels. For Vehicle #1 (Figure 7a), the PN EFs were higher in the WLTC cycle than in the NEDC cycle. The reason for this is that the vehicle had a higher average speed, a higher engine load, and more frequent acceleration and deceleration. This led to the incomplete combustion of fuel, thus generating many particles. At the same time, the high fuel consumption of Vehicle #1 under WLTC conditions is also one of the reasons for emissions. In the NEDC test cycle, fuels with a high RON emitted more particles, and the EF of particle number was lower with ethanol–gasoline. G3 emitted the most TPN (1.4×10^{12} #/km) and E1 had the lowest TPN EF (9.9×10^{11} #/km). The proportion of nucleation-mode particles produced by high-RON fuels was lower than that produced by low-RON fuels. On the contrary, high-RON fuel produced a higher proportion of accumulation-mode particles. The proportions of nucleation-mode particles were 84.02%, 83.58%, 82.42%, 81.36%, 73.93%, and 73.48%, respectively, for the six fuels, and the proportions of accumulation-mode particles were 15.98%, 16.34%, 17.55%, 18.63%, 26.06%, and 26.52%, respectively. Similarly, fuels with a high RON produced less PN in the WLTC. The EF of TPN was the highest for G2 fuel (3.4×10^{13} #/km), and E2 had the lowest EF (1.7×10^{13} #/km). The difference in the proportion of nucleation-mode particulates and accumulation-mode particles produced by high-RON fuel compared with low-RON fuel was small. The proportions of nucleation-mode particles were 94.95%, 97.63%, 97.49%, 96.82%, 97.14%, and 96.29%, respectively. The proportions of accumulation-mode particles are 5.01%, 2.35%, 2.49%, 3.16%, 2.83%, and 3.69%, respectively. Although the EF of accumulation-mode particles was very low in the WLTC, it was still higher than that of the NEDC. Compared with the TPN EFs of the two test cycles, the TPN EF of the WLTC was an order of magnitude higher than that of the NEDC.

For Vehicle #2 (Figure 7b), the difference in PN EF between the two test cycles was small. During the NEDC test cycle, high-RON fuels produced higher PN EFs. E2 fuel had the highest PN EF (2.7×10^{12} #/km), while G1 had the lowest EF (1.9×10^{12} #/km). Compared with traditional gasoline, the proportion of nucleation-mode particulates emitted by ethanol–gasoline was higher but the proportion of accumulation-mode particulates was lower. The proportions of nucleation-mode particles were 76.14%, 69.64%, 77.47%, 76.87%, 71.15%, and 79.74%, respectively. The proportions of accumulation-mode particles were 23.86%, 30.36%, 22.51%, 23.13%, 28.84%, and 20.26%, respectively. In the same way, fuels with a high RON produce more PN in the WLTC. The EF of TPN was the highest for E2 fuel (2.9×10^{12} #/km), and G1 had the lowest EF (1.7×10^{12} #/km). The difference in the proportion of nucleation-mode particulates and accumulation-mode particles produced by high RON fuel compared with low RON fuel was small. The proportions of nucleation-mode particles were 75.64%, 72.41%, 77.65%, 78.75%, 74.39%, and 78.87%, respectively. The proportions of accumulation-mode particles were 24.36%, 27.59%, 22.35%, 21.22%, 25.58%, and 21.16%, respectively. There was little difference in the TPN EF between the two test cycles, and those of the WLTC were -7.31% , 7.28% , 7.21% , 31.92% , 9.71% , and 2.74% higher than those of the NEDC for the six fuels, respectively.

3.4.3. PSD Analysis

Figure S9a shows the PSD of Vehicle #1 during the NEDC and WLTC cycles with the six fuels. During the NEDC, the PSD demonstrated a bimodal logarithmic distribution, and two nucleation particle number concentration peaks appeared around 16 nm and

40 nm. The particle number concentration was 10^6 #/cm³ at the position of the two peaks. Interestingly, at the first peak, high-RON fuels (G3, G4, and E2) produced fewer particles than low-RON fuels, and G2 had the highest PN concentration (1.2×10^6 #/cm³). However, at the second peak, high-RON fuels emitted more PN, and G3 had the highest PN concentration (1.7×10^6 #/cm³). During the WLTC cycle, the PSD demonstrated a unimodal logarithmic distribution, and the peak corresponded to a particle size of about 16 nm, similar to the first peak for the NEDC. The particle number concentration was 10^7 #/cm³ at the peak position, and E1 had the highest PN concentration (4×10^7 #/cm³). The PN concentration decreased sharply when the particle size was larger than 140 nm, and when the particle sizes were in the range of 300–1000 nm, the particle number concentration is 10 #/cm³ and 10^3 #/cm³ at NEDC and WLTC.



(a)

Figure 7. Cont.

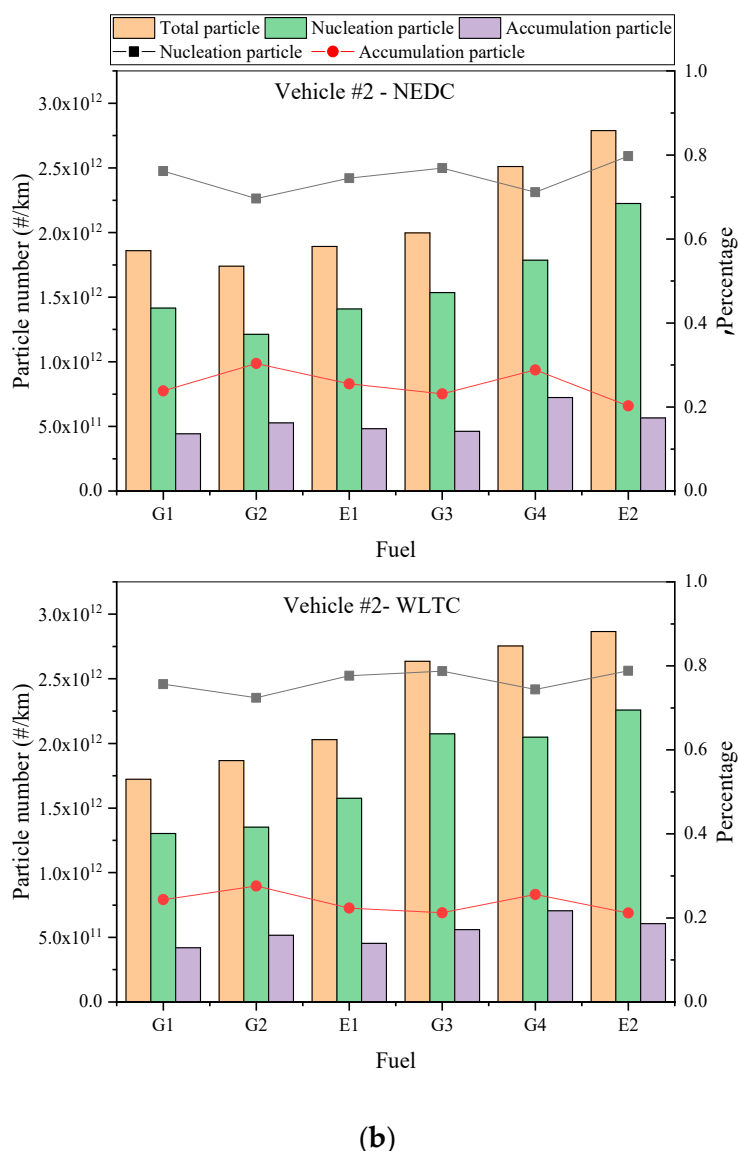


Figure 7. Particle number EFs of the two vehicles during the NEDC and WLTC test cycles: (a) Vehicle #1; (b) Vehicle #2.

Figure S9b shows the PSDs of Vehicle #2 during the NEDC and WLTC cycles with the six fuels. Unlike Vehicle #1, the PN concentration gap for different particle sizes between the NEDC and WLTC was tiny for Vehicle #2. The PSDs of the six fuels all appeared to have a bimodal logarithmic distribution during the two test cycles, and the two peaks appeared around 18 nm and 42 nm. High-RON fuels (G3, G4, E2) produced more particles than low-RON fuels. At the first peak position, E2 had the highest PN concentration during the NEDC and WLTC: $4.7 \times 10^6 \text{ #/cm}^3$ for the NEDC and $4.2 \times 10^6 \text{ #/cm}^3$ for the WLTC. At the second peak position, G4 had the highest PN concentration ($3.3 \times 10^6 \text{ #/cm}^3$) for the NEDC, and G3 had the highest PN concentration ($4.1 \times 10^6 \text{ #/cm}^3$) for the WLTC. The PN concentration decreased sharply when the particle size was larger than 150 nm. When the particle size was located in the range of 300–1000 nm, the particle number concentration was 10 #/cm^3 and 100 #/cm^3 for the NEDC and WLTC, respectively. Hu et al. tested the PSD of gasoline direct injection vehicles, and also found a bimodal distribution, but the peak particle size (at 6 and 50 nm in diameter) was different from that in this study [59]. Tan et al. tested the particle size distribution of diesel vehicles, and also found that bimodal distribution with the peak particle sizes are about 10 nm and 50 nm [60]. However, the

maximum concentration of PN emitted by diesel vehicles can reach 10^9 \#/cm^3 , which is significantly higher than that of the gasoline vehicles in this study.

Figure 8 shows that the EFs of different particle sizes based on the two test vehicles' driving distance, the distribution of the emission concentrations, and the emission factors of particles with different sizes, were similar [59]. The PN EFs for Vehicle #1 with different particle sizes are shown in Figure 8a. For the NEDC cycle, all test fuels' particle size distribution characteristics present similar bimodal distributions, with two peaks at 18 nm and 40 nm in diameter. G2 had the highest PN EF ($6.7 \times 10^{10} \text{ \#/km}$) at the first peak, and G3 had the highest EF ($8.1 \times 10^{10} \text{ \#/km}$) at the second peak. During the WLTC, the PSD demonstrated a unimodal logarithmic distribution (the particle size was 16 nm), and G2 produced the highest EF ($4 \times 10^{12} \text{ \#/km}$) at the peak. Figure 8b demonstrates the PN EFs of Vehicle #2 with different particle sizes. The six fuels' PSDs appear to have a bimodal logarithmic distribution during the two test cycles (the two peaks appeared at around 18 nm and 42 nm). At the first peak, E2 had the highest PN EF during the NEDC and WLTC: $1.7 \times 10^{11} \text{ \#/km}$ for the NEDC and $1.8 \times 10^{11} \text{ \#/km}$ for the WLTC. At the second peak, G4 had the highest PN EF ($1.2 \times 10^{11} \text{ \#/km}$) for the NEDC cycle, and G3 had the highest PN EF ($1.3 \times 10^{11} \text{ \#/km}$) for the WLTC cycle. By and large, fuels with a higher RON emit more small particles in Vehicle #2. The test results of this study are higher than those of other studies [59].

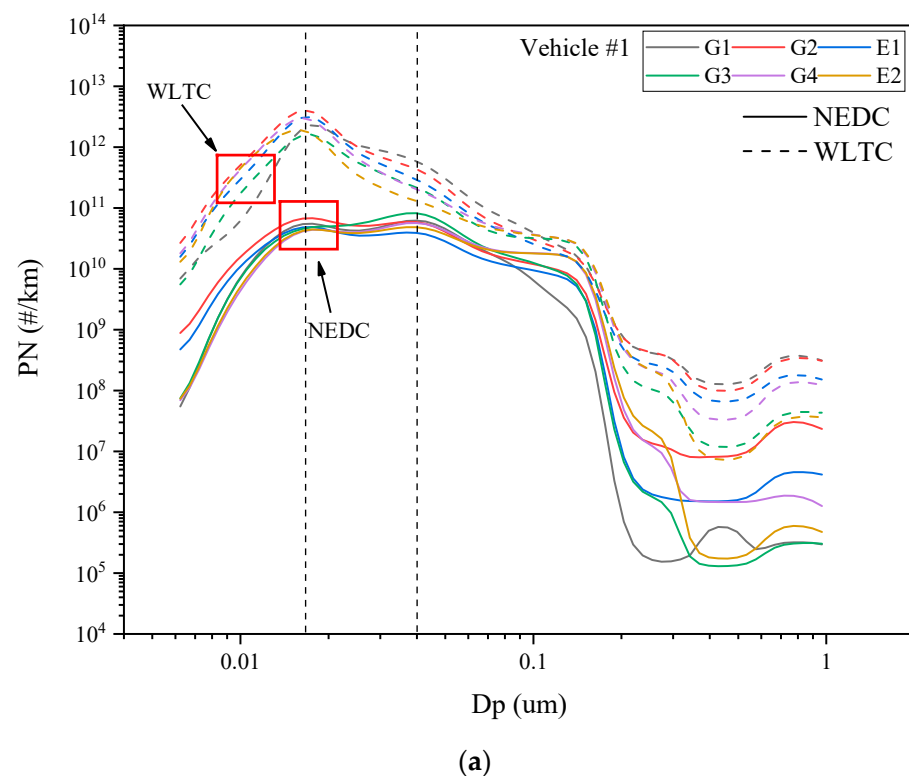


Figure 8. Cont.

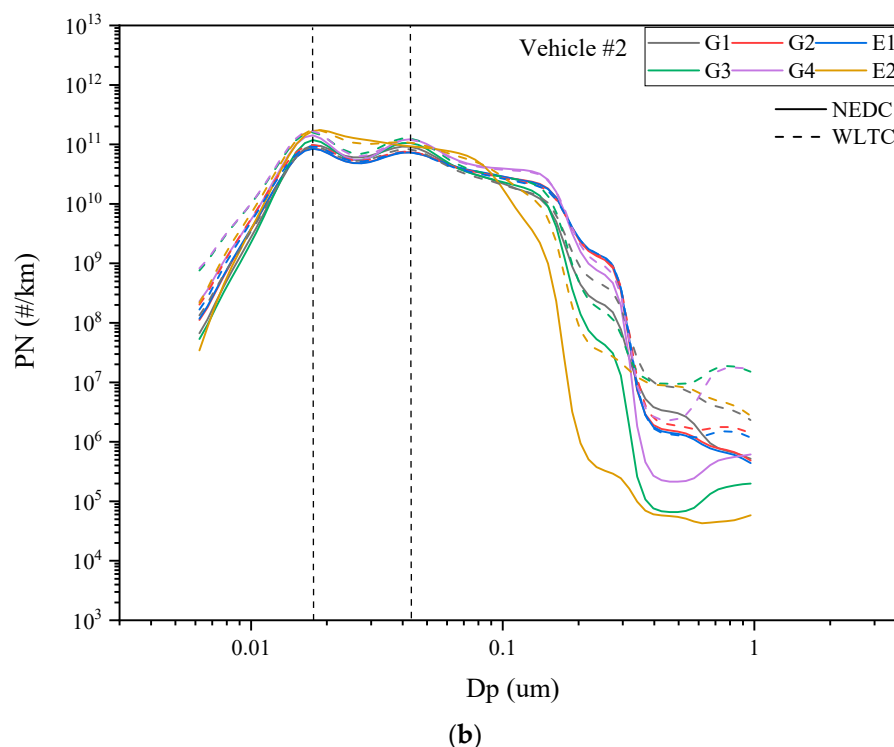


Figure 8. EFs of particles with different particle sizes: (a) Vehicle #1; (b) Vehicle #2.

3.4.4. Discussion of Particulate Emission

Generally, the PN EFs of the WLTC were higher than those of the NEDC because the WLTC cycle has a higher average speed, more frequent acceleration, and higher fuel consumption. Vehicle #1 fully confirmed this conclusion, but Vehicle #2 did not. According to the working conditions of the vehicles' engine in the test processes, Vehicle #1 had a lower average engine speed and a higher average engine load. This led to an unstable combustion process and worse combustion conditions, resulting in large amounts of particulate matter being generated (mostly NPM). In contrast, the engine load of Vehicle #2 was relatively low and changed slightly during the WLTC cycle, resulting in little variation between the NEDC and WLTC cycles.

Different engines must use the appropriate fuel to run better and generate lower emissions. From the point of view of PN emissions alone, Vehicle #1 was more suitable for low-RON fuel, while Vehicle #2 was more suitable for high-RON fuel. The higher the olefin and aromatic hydrocarbon content of fuels with the same RON, the more particles will be emitted (G2 has a higher olefin and aromatic content than G1, and G4 has a higher olefin and aromatic content than G3). For Vehicle #1 with a higher average engine load, ethanol-gasoline emitted less PN than conventional gasoline. In contrast, for Vehicle #2 (high engine speed and low load), ethanol-gasoline emitted more PN. In summary, the main factor affecting PN emissions is the engine parameters.

3.5. Matching of Vehicles and Fuels

In this section, the fuel consumption and pollutant emission factors of the two vehicles using six kinds of fuel under two test conditions are compared and analyzed comprehensively by using radar charts, as shown in Figure 9. The fuel consumption and pollutant emission factors of each fuel were normalized to evaluate the adaptability of the vehicle to the fuel, which is helpful for finding out the better fuel match for the vehicle. As shown in the figure, the change in fuel performance has little influence on CO₂ and fuel consumption but had strong influence on other pollutants.

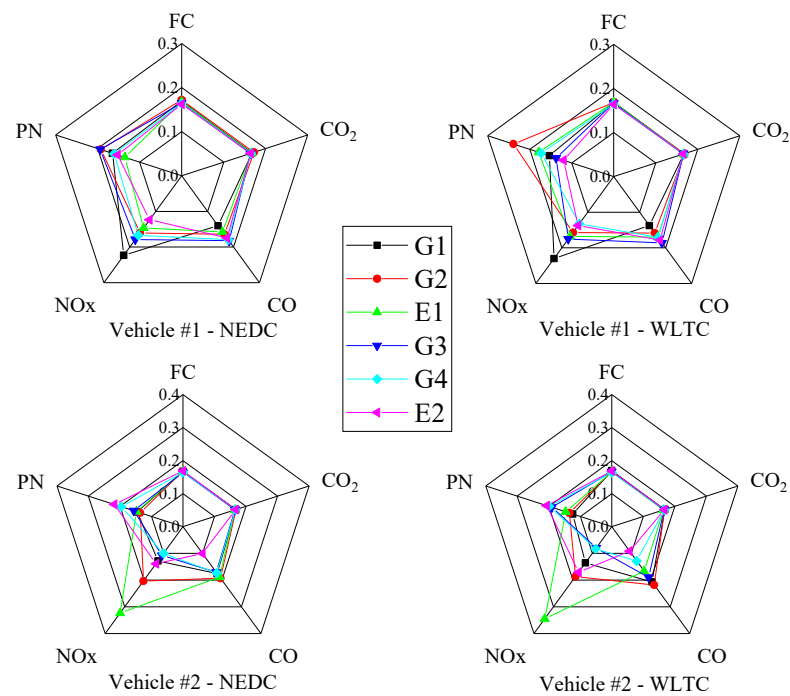


Figure 9. Radar chart of normalized pollutant emission factor.

Lower-RON gasoline will lead to more intense combustion in the engine, resulting in a higher combustion temperature. Ethanol–gasoline is an oxygen-enriched fuel, which can promote the complete combustion of fuel. Therefore, lower-RON ethanol–gasoline may lead to higher NO_x emissions and lower PN and CO. As shown in the figure, for Vehicle #1, the NO_x emissions of low-RON fuel were higher, but the NO_x emissions of ethanol–fuel were lower. It was found that the PN and CO emissions of ethanol–gasoline with low RON were lower during the NEDC test cycle. However, under the WLTC test condition, the PN emissions of low-RON fuel were higher. For Vehicle #2, the difference in the pollutants emitted by different fuels under the two test cycles was exceedingly small. Low-RON fuel produced more PN and CO, which is different from the result for Vehicle #1. Moreover, the NO_x emissions of ethanol–gasoline with a low RON were significantly higher than those of other fuels.

Many studies suggest that the WLTC test conditions are more in line with the actual road driving characteristics of motor vehicles. Therefore, by calculating a comprehensive index (the area of the radar map, as shown in Table S1) of each fuel, the optimal matching fuel for the two vehicles is obtained. E2 is the most suitable for Vehicle #1, and G4 is the most suitable for Vehicle #2. At present, China is vigorously promoting ethanol–gasoline nationwide, and many cities have stopped selling traditional gasoline. Based on the research in this paper, ethanol–gasoline with a high RON is a good choice for Vehicle #1 (Euro 5), but Vehicle #2 (Euro 6) is more suitable for the use of traditional gasoline with a high RON. At present, China is vigorously promoting ethanol–gasoline, but not all vehicles using ethanol–gasoline can achieve the purpose of emission reduction. Therefore, the promotion of new vehicles and fuel should be based on experimental support in the future.

4. Conclusions

In this study, the effects of the performance of different fuel (RON and ethanol content) and engine operation characteristics on the gaseous pollutants and particulate emissions from two light passenger vehicles were experimentally investigated. The results are summarized as follows:

- (1) Compared with the NEDC test cycle, the test vehicles had higher fuel consumption and pollutant emission factors during the WLTC test cycle. For Vehicle #1, the fuel

- consumption and emission factors for the WLTC cycle were significantly higher than those under the NEDC test conditions. For Vehicle #2, the fuel consumption and emission factors for the WLTC were also higher than those under the NEDC test conditions, but the gap was exceedingly small;
- (2) Fuel performance will affect vehicle emissions. The content of olefins and aromatics has little effect on emissions, but RON and ethanol content have a strong impact on emissions. An increase in RON led to an increase in fuel economy and a decrease in NO_x emissions for the two vehicles. For vehicle #1, increasing the RON led to higher CO emissions and lower PN emissions. For Vehicle #2, the observation was the opposite. When ethanol–gasoline was used, the CO and PN emissions increased and the NO_x emissions decreased for Vehicle #1, while the CO emissions decreased and the NO_x and PN emissions increased for Vehicle #2. For the four traditional fuels, increasing the fuel's aromatic content led to higher particle number emissions;
 - (3) Many particles are emitted during the driving process, of which the largest proportion is that of the nucleation-mode particles. For Vehicle #1, the proportion of nucleation-mode particles was between 70% and 90%. For Vehicle #2, the proportion of nucleation-mode particles was higher, more than 90%. There were two peaks in the particle emission particle size distribution, at about 18 nm and 40 nm;
 - (4) From the perspective of emissions levels, the adaptability of the two vehicles to six kinds of fuel was analyzed. Through a comparative analysis, the fuel suitable for the test vehicle in this study was found. The Euro 6 vehicle (Vehicle #2) in this experiment is more suitable for the use of traditional gasoline with a high RON.

Supplementary Materials: The following supporting information can be downloaded at: <https://www.mdpi.com/article/10.3390/en15020622/s1>, Figure S1: Schematic diagram of the test system; Figure S2: Acceleration VS vehicle speed for the NEDC and WLTC test cycles; Figure S3: Time-solved profiles of vehicle' speed, acceleration, and corresponding engine' speed, load; Figure S4: Time evolution of the CO₂ during the test cycles with eight different test fuels of the two vehicles; Figure S5: Time evolution of the instantaneous fuel consumption rate during the test cycles with eight different test fuels of the two vehicles; Figure S6: Time evolution of the CO during the test cycles with eight different test fuels of the two vehicles; Figure S7: Time evolution of the NO_x during the test cycles with eight different test fuels of the two vehicles; Figure S8: Instantaneous particle number concentration from the two vehicles during the NEDC and WLTC with different fuels; Figure S9: The number concentration of particles with different particle sizes; Table S1. The area of each pentagon in the radar chart (Figure 9).

Author Contributions: The contributions of the authors are summarized as follows: conceptualization, Q.Z., H.M. and Z.L.; methodology, L.Y. and M.S.; software, J.M.; investigation, L.Y.; data curation, Z.L. and L.Y.; writing—original draft preparation, Z.L.; writing—review and editing, L.W. and J.P.; visualization, Z.L.; supervision, L.W. and H.M.; project administration, J.P. and Q.Z. All authors have read and agreed to the published version of the manuscript.

Funding: This research received no external funding.

Acknowledgments: This work is funded by the National Natural Science Foundation of China (21607081), the Tianjin Science and Technology Plan Project (20YFZCSN01000, 19YFZCSF00960), and the Tianjin Science and Technology Project (20JCYBJC01270).

Conflicts of Interest: The authors declare no conflict of interest.

References

1. Zhang, Y.; Baltensperger, U.; Schnelle-Kreis, J.; An, Z.; Han, Y.; Crippa, M.; Zotter, P.; Platt, S.M.; Cao, J.-J.; Ho, K.-F.; et al. High secondary aerosol contribution to particulate pollution during haze events in China. *Nature* **2014**, *514*, 218–222.
2. Schifter, I.; Diaz, L.; Gonzalez, U.; Macias, U.G. Fuel formulation for recent model light duty vehicles in Mexico base on a model for predicting gasoline emissions. *Fuel* **2013**, *107*, 371–381. [[CrossRef](#)]
3. Fushimi, A.; Kondo, Y.; Kobayashi, S.; Fujitani, Y.; Saitoh, K.; Takami, A.; Tanabe, K. Chemical composition and source of fine and nanoparticles from recent direct injection gasoline passenger cars: Effects of fuel and ambient temperature. *Atmos. Environ.* **2016**, *124*, 77–84. [[CrossRef](#)]

4. Awad, O.I.; Ma, X.; Kamil, M.; Ali, O.M.; Zhang, Z.; Shuai, S. Particulate emissions from gasoline direct injection engines: A review of how current emission regulations are being met by automobile manufacturers. *Sci. Total Environ.* **2020**, *718*, 137302. [[CrossRef](#)]
5. Yang, J.; Roth, P.; Zhu, H.; Durbin, T.D.; Karavalakis, G. Impacts of gasoline aromatic and ethanol levels on the emissions from GDI vehicles: Part 2. Influence on particulate matter, black carbon, and nanoparticle emissions. *Fuel* **2019**, *252*, 812–820. [[CrossRef](#)]
6. Sayin, C.; Kilicaslan, I.; Canakci, M.; Ozsezen, N. An experimental study of the effect of octane number higher than engine requirement on the engine performance and emissions. *Appl. Therm. Eng.* **2005**, *25*, 1315–1324. [[CrossRef](#)]
7. Binjuwair, S.; Mohamad, T.I.; Almaleki, A.; Alkudsi, A.; Alshunaifi, I. The effects of research octane number and fuel systems on the performance and emissions of a spark ignition engine: A study on Saudi Arabian RON91 and RON95 with port injection and direct injection systems. *Fuel* **2015**, *158*, 351–360. [[CrossRef](#)]
8. Liu, H.; Yao, M.; Zhang, B.; Zheng, Z. Effects of Inlet Pressure and Octane Numbers on Combustion and Emissions of a Homogeneous Charge Compression Ignition (HCCI) Engine. *Energy Fuels* **2008**, *22*, 2207–2215. [[CrossRef](#)]
9. Broustail, G.; Halter, F.; Seers, P.; Moréac, G.; Mounaim-Rousselle, C. Comparison of regulated and non-regulated pollutants with iso-octane/butanol and iso-octane/ethanol blends in a port-fuel injection Spark-Ignition engine. *Fuel* **2012**, *94*, 251–261. [[CrossRef](#)]
10. Lattimore, T.; Herreros, J.M.; Xu, H.; Shuai, S. Investigation of compression ratio and fuel effect on combustion and PM emissions in a DISI engine. *Fuel* **2016**, *169*, 68–78. [[CrossRef](#)]
11. Iodice, P.; Langella, G.; Amoresano, A. Ethanol in gasoline fuel blends: Effect on fuel consumption and engine out emissions of SI engines in cold operating conditions. *Appl. Therm. Eng.* **2018**, *130*, 1081–1089. [[CrossRef](#)]
12. Catapano, F.; Sementa, P.; Vaglieco, B.M. Air-fuel mixing and combustion behavior of gasoline-ethanol blends in a GDI wall-guided turbocharged multi-cylinder optical engine. *Renew. Energy* **2016**, *96*, 319–332. [[CrossRef](#)]
13. Jin, D.; Choi, K.; Myung, C.-L.; Lim, Y.; Lee, J.; Park, S. The impact of various ethanol-gasoline blends on particulates and unregulated gaseous emissions characteristics from a spark ignition direct injection (SIDI) passenger vehicle. *Fuel* **2017**, *209*, 702–712. [[CrossRef](#)]
14. Maricq, M.M.; Szente, J.J.; Jahr, K. The Impact of Ethanol Fuel Blends on PM Emissions from a Light-Duty GDI Vehicle. *Aerosol Sci. Technol.* **2012**, *46*, 576–583. [[CrossRef](#)]
15. Karavalakis, G.; Short, D.; Russell, R.L.; Jung, H.; Johnson, K.C.; Asa-Awuku, A.; Durbin, T.D. Assessing the impacts of ethanol and isobutanol on gaseous and particulate emissions from flexible fuel vehicles. *Environ. Sci. Technol.* **2014**, *48*, 14016–14024. [[CrossRef](#)]
16. Fatouraie, M.; Wooldridge, M.S.; Petersen, B.R.; Wooldridge, S.T. Effects of Ethanol on In-Cylinder and Exhaust Gas Particulate Emissions of a Gasoline Direct Injection Spark Ignition Engine. *Energy Fuels* **2015**, *29*, 3399–3412. [[CrossRef](#)]
17. Wu, J.; Song, K.H.; Litzinger, T.; Lee, S.-Y.; Santoro, R.; Linevsky, M.; Colket, M.; Liscinsky, D. Reduction of PAH and soot in premixed ethylene-air flames by addition of ethanol. *Combust. Flame* **2006**, *144*, 675–687. [[CrossRef](#)]
18. Lemaire, R.; Therssen, E.; Desgroux, P. Effect of ethanol addition in gasoline and gasoline–surrogate on soot formation in turbulent spray flames. *Fuel* **2010**, *89*, 3952–3959. [[CrossRef](#)]
19. Khosousi, A.; Liu, F.; Dworkin, S.B.; Eaves, N.A.; Thomson, M.J.; He, X.; Dai, Y.; Gao, Y.; Liu, F.; Shuai, S.; et al. Experimental and numerical study of soot formation in laminar coflow diffusion flames of gasoline/ethanol blends. *Combust. Flame* **2015**, *162*, 3925–3933. [[CrossRef](#)]
20. Yang, J.; Roth, P.; Durbin, T.D.; Johnson, K.C.; Asa-Awuku, A.; Cocker, D.R.; Karavalakis, G. Investigation of the Effect of Mid-And High-Level Ethanol Blends on the Particulate and the Mobile Source Air Toxic Emissions from a Gasoline Direct Injection Flex Fuel Vehicle. *Energy Fuels* **2018**, *33*, 429–440. [[CrossRef](#)]
21. Chen, L.; Stone, R.; Richardson, D. A study of mixture preparation and PM emissions using a direct injection engine fuelled with stoichiometric gasoline/ethanol blends. *Fuel* **2012**, *96*, 120–130. [[CrossRef](#)]
22. Storch, M.; Koegl, M.; Altenhoff, M.; Will, S.; Zigan, L. Investigation of soot formation of spark-ignited ethanol-blended gasoline sprays with single- and multi-component base fuels. *Appl. Energy* **2016**, *181*, 278–287. [[CrossRef](#)]
23. Leach, F.C.; Stone, R.; Richardson, D.; Turner, J.W.; Lewis, A.; Akehurst, S.; Remmert, S.; Campbell, S.; Cracknell, R. The effect of oxygenate fuels on PN emissions from a highly boosted GDI engine. *Fuel* **2018**, *225*, 277–286. [[CrossRef](#)]
24. Vuk, C.; Vander Griend, S.J. Fuel Property Effects on Particulates in Spark Ignition Engines. *SAE Tech. Pap. Ser.* **2013**, *2*, 1124.
25. Chen, L.; Zhang, Z.; Gong, W.; Liang, Z. Quantifying the effects of fuel compositions on GDI-derived particle emissions using the optimal mixture design of experiments. *Fuel* **2015**, *154*, 252–260. [[CrossRef](#)]
26. Karavalakis, G.; Short, D.; Vu, D.; Russell, R.; Hajbabaie, M.; Asa-Awuku, A.; Durbin, T.D. Evaluating the Effects of Aromatics Content in Gasoline on Gaseous and Particulate Matter Emissions from SI-PFI and SIDI Vehicles. *Environ. Sci. Technol.* **2015**, *49*, 7021–7031. [[CrossRef](#)]
27. Wang, Y.; Zheng, R.; Qin, Y.; Peng, J.; Li, M.; Lei, J.; Wu, Y.; Hu, M.; Shuai, S. The impact of fuel compositions on the particulate emissions of direct injection gasoline engine. *Fuel* **2016**, *166*, 543–552.
28. Zhu, R.; Hu, J.; Bao, X.; He, L.; Zu, L. Effects of aromatics, olefins and distillation temperatures (T50 & T90) on particle mass and number emissions from gasoline direct injection (GDI) vehicles. *Energy Policy* **2017**, *101*, 185–193.
29. Yang, J.; Roth, P.; Durbin, T.; Karavalakis, G. Impacts of gasoline aromatic and ethanol levels on the emissions from GDI vehicles: Part 1. Influence on regulated and gaseous toxic pollutants. *Fuel* **2019**, *252*, 799–811. [[CrossRef](#)]

30. Schifter, I.; Díaz, L.; Sánchez-Reyna, G.; Macias, U.G.; González, U.; Rodríguez, R. Influence of gasoline olefin and aromatic content on exhaust emissions of 15% ethanol blends. *Fuel* **2020**, *265*, 116950. [[CrossRef](#)]
31. Han, Y.; Hu, S.; Sun, Y.; Sun, X.; Tan, M.; Xu, Y.; Tian, J.; Li, R.; Shao, Z. Compositional Effect of Gasoline on Fuel Economy and Emissions. *Energy Fuels* **2018**, *32*, 5072–5080. [[CrossRef](#)]
32. Yao, C.; Dou, Z.; Wang, B.; Liu, M.; Lu, H.; Feng, J.; Feng, L. Experimental study of the effect of heavy aromatics on the characteristics of combustion and ultrafine particle in DISI engine. *Fuel* **2017**, *203*, 290–297. [[CrossRef](#)]
33. Chan, T.W.; Lax, D.; Gunter, G.C.; Hendren, J.; Kubsh, J.; Brezny, R. Assessment of the Fuel Composition Impact on Black Carbon Mass, Particle Number Size Distributions, Solid Particle Number, Organic Materials, and Regulated Gaseous Emissions from a Light-Duty Gasoline Direct Injection Truck and Passenger Car. *Energy Fuels* **2017**, *31*, 10452–10466. [[CrossRef](#)]
34. Leach, F.C.; Stone, R.; Richardson, D.; Lewis, A.G.; Akehurst, S.; Turner, J.W.; Shankar, V.; Chahal, J.; Cracknell, R.F.; Aradi, A. The effect of fuel composition on particulate emissions from a highly boosted GDI engine—An evaluation of three particulate indices. *Fuel* **2019**, *252*, 598–611. [[CrossRef](#)]
35. Chen, L.; Liang, Z.; Zhang, X.; Shuai, S. Characterizing particulate matter emissions from GDI and PFI vehicles under transient and cold start conditions. *Fuel* **2017**, *189*, 131–140. [[CrossRef](#)]
36. Bonatesta, F.; Chiappetta, E.; La Rocca, A. Part-load particulate matter from a GDI engine and the connection with combustion characteristics. *Appl. Energy* **2014**, *124*, 366–376. [[CrossRef](#)]
37. Raza, M.; Chen, L.; Leach, F.; Ding, S. A Review of Particulate Number (PN) Emissions from Gasoline Direct Injection (GDI) Engines and Their Control Techniques. *Energies* **2018**, *11*, 1417. [[CrossRef](#)]
38. Conte, M.; Contini, D. Size-resolved particle emission factors of vehicular traffic derived from urban eddy covariance measurements. *Environ. Pollut.* **2019**, *251*, 830–838. [[CrossRef](#)] [[PubMed](#)]
39. Rönkkö, T.; Kuuluvainen, H.; Karjalainen, P.; Keskinen, J.; Hillamo, R.; Niemi, J.; Pirjola, L.; Timonen, H.J.; Saarikoski, S.; Saukko, E.; et al. Traffic is a major source of atmospheric nanocluster aerosol. *Proc. Natl. Acad. Sci. USA* **2017**, *114*, 7549–7554. [[CrossRef](#)]
40. Hooftman, N.; Messagie, M.; Van Mierlo, J.; Coosemans, T. A review of the European passenger car regulations—Real driving emissions vs local air quality. *Renew. Sustain. Energy Rev.* **2018**, *86*, 1–21. [[CrossRef](#)]
41. Pavlovic, J.; Marotta, A.; Ciuffo, B. CO₂ emissions and energy demands of vehicles tested under the NEDC and the new WLTP type approval test procedures. *Appl. Energy* **2016**, *177*, 661–670. [[CrossRef](#)]
42. Karagöz, Y. Analysis of the impact of gasoline, biogas and biogas + hydrogen fuels on emissions and vehicle performance in the WLTC and NEDC. *Int. J. Hydrog. Energy* **2019**, *44*, 31621–31632. [[CrossRef](#)]
43. Sileghem, L.; Bosteels, D.; May, J.; Favre, C.; Verhelst, S. Analysis of vehicle emission measurements on the new WLTC, the NEDC and the CADC. *Transp. Res. Part D Transp. Environ.* **2014**, *32*, 70–85. [[CrossRef](#)]
44. Dimaratos, A.; Tsokolis, D.; Fontaras, G.; Tsiakmakis, S.; Ciuffo, B.; Samaras, Z. Comparative Evaluation of the Effect of Various Technologies on Light-duty Vehicle CO₂ Emissions over NEDC and WLTP. *Transp. Res. Procedia* **2016**, *14*, 3169–3178. [[CrossRef](#)]
45. Marotta, A.; Pavlovic, J.; Ciuffo, B.; Serra, S.; Fontaras, G. Gaseous Emissions from Light-Duty Vehicles: Moving from NEDC to the New WLTP Test Procedure. *Environ. Sci. Technol.* **2015**, *49*, 8315–8322. [[CrossRef](#)]
46. Demuyneck, J.; Bosteels, D.; De Paepe, M.; Favre, C.; May, J.; Verhelst, S. Recommendations for the new WLTP cycle based on an analysis of vehicle emission measurements on NEDC and CADC. *Energy Policy* **2012**, *49*, 234–242. [[CrossRef](#)]
47. Wang, Y.; Hao, C.; Ge, Y.; Hao, L.; Tan, J.; Wang, X.; Zhang, P.; Wang, Y.; Tian, W.; Lin, Z.; et al. Fuel consumption and emission performance from light-duty conventional/hybrid-electric vehicles over different cycles and real driving tests. *Fuel* **2020**, *278*, 118340. [[CrossRef](#)]
48. Grigoratos, T.; Fontaras, G.; Giechaskiel, B.; Zacharof, N. Real world emissions performance of heavy-duty Euro VI diesel vehicles. *Atmos. Environ.* **2019**, *201*, 348–359. [[CrossRef](#)]
49. Yli-Ojanperä, J.; Kannosto, J.; Marjamäki, M.; Keskinen, J. Improving the Nanoparticle Resolution of the ELPI. *Aerosol Air Qual. Res.* **2010**, *10*, 360–366. [[CrossRef](#)]
50. Järvinen, A.; Aitomaa, M.; Rostedt, A.; Keskinen, J.; Yli-Ojanperä, J. Calibration of the new electrical low pressure impactor (ELPI+). *J. Aerosol Sci.* **2014**, *69*, 150–159. [[CrossRef](#)]
51. Zervas, E.; Dorlhene, P. Comparison of Exhaust Particle Number Measured by EEPS, CPC, and ELPI. *Aerosol Sci. Technol.* **2006**, *40*, 977–984. [[CrossRef](#)]
52. Saari, S.; Arffman, A.; Harra, J.; Rönkkö, T.; Keskinen, J. Performance evaluation of the HR-ELPI + inversion. *Aerosol Sci. Technol.* **2018**, *52*, 1037–1047. [[CrossRef](#)]
53. Lepistö, T.; Kuuluvainen, H.; Juuti, P.; Järvinen, A.; Arffman, A.; Rönkkö, T. Measurement of the human respiratory tract deposited surface area of particles with an electrical low pressure impactor. *Aerosol Sci. Technol.* **2020**, *54*, 958–971. [[CrossRef](#)]
54. Kittelson, D.B. Engines and nanoparticles: A review. *J. Aerosol Sci.* **1998**, *29*, 575–588. [[CrossRef](#)]
55. Sun, W.; Wang, Q.; Guo, L.; Cheng, P.; Li, D.; Yan, Y. Influence of biodiesel/diesel blends on particle size distribution of CI engine under steady/transient conditions. *Fuel* **2019**, *245*, 336–344. [[CrossRef](#)]
56. Zhou, J.; Cheung, C.; Zhao, W.; Leung, C. Diesel-hydrogen dual-fuel combustion and its impact on unregulated gaseous emissions and particulate emissions under different engine loads and engine speeds. *Energy* **2016**, *94*, 110–123. [[CrossRef](#)]
57. Man, X.; Cheung, C.S.; Ning, Z.; Wei, L.; Huang, Z. Influence of engine load and speed on regulated and unregulated emissions of a diesel engine fueled with diesel fuel blended with waste cooking oil biodiesel. *Fuel* **2016**, *180*, 41–49. [[CrossRef](#)]

58. Stradling, R.; Williams, J.; Hamje, H.; Rickeard, D. Effect of Octane on Performance, Energy Consumption and Emissions of Two Euro 4 Passenger Cars. *Transp. Res. Procedia* **2016**, *14*, 3159–3168. [[CrossRef](#)]
59. Hu, Z.; Lu, Z.; Song, B.; Quan, Y. Impact of test cycle on mass, number and particle size distribution of particulates emitted from gasoline direct injection vehicles. *Sci. Total Environ.* **2020**, *762*, 143128. [[CrossRef](#)]
60. Tan, P.-Q.; Li, Y.; Hu, Z.-Y.; Lou, D.-M. Investigation of nitrogen oxides, particle number, and size distribution on a light-duty diesel car with B10 and G10 fuels. *Fuel* **2017**, *197*, 373–387. [[CrossRef](#)]